

First-principles study of As interstitials in GaAs: Convergence, relaxation, and formation energy

J. T. Schick*

Physics Department, Villanova University, Villanova, PA 19085, USA

C. G. Morgan and P. Papoulias

Department of Physics and Astronomy, Wayne State University, Detroit, MI 48202, USA

(Dated: August 19, 2002)

Convergence of density-functional supercell calculations for defect formation energies, charge transition levels, localized defect state properties, and defect atomic structure and relaxation is investigated using the arsenic split interstitial in GaAs as an example. Supercells containing up to 217 atoms and a variety of \mathbf{k} -space sampling schemes are considered. It is shown that a good description of the localized defect state dispersion and charge state transition levels requires at least a 217-atom supercell, although the defect structure and atomic relaxations can be well converged in a 65-atom cell. Formation energies are calculated for the As split interstitial, Ga vacancy, and As antisite defects in GaAs, taking into account the dependence upon chemical potential and Fermi energy. It is found that equilibrium concentrations of As interstitials will be much lower than equilibrium concentrations of As antisites in As-rich, n -type or semi-insulating GaAs.

PACS numbers: 61.72.Bb, 61.72.Ji, 71.55.-i

I. INTRODUCTION

Interstitials are the most complicated of the simple point defects, and the most elusive. For example, even though arsenic interstitials must be created by irradiation of GaAs with sufficiently energetic particles, and they can subsequently be observed to recombine with arsenic vacancies when the sample is heated above 220° C, isolated arsenic interstitials have not been observed directly in EPR, electrical, or optical experiments.¹

It has been argued based on a thorough analysis²⁻⁴ of a variety of experimental data including titration experiments⁵ and measurements of density and lattice parameter⁶ that melt-grown GaAs is always As-rich unless the concentration of Ga in the melt is substantially greater than 50%, and that this deviation from stoichiometry is due primarily to the creation of large numbers of As interstitials (As_i) during growth. In particular, Hurle has argued² that the measured deviation of the mass per unit cell as a function of arsenic concentration in the melt must be explained by arsenic interstitials and/or arsenic vacancies, since the number of arsenic antisites which would be required to fit the data is unrealistically large (up to several percent), due to the small difference between the atomic masses of arsenic and gallium. Hurle's work also contains an extensive thermodynamic analysis, including estimates of the mass action constants for the formation of all the neutral native point defects. These estimates are derived by fitting to a large quantity of experimental data on both doped and undoped GaAs, under the assumption that native defect and dopant concentrations are near equilibrium close to the melting point and during high temperature growth from the melt or from solution.

In the high temperature growth regime, observations of defects tentatively described as high concentrations

or diffuse 'clouds' of arsenic interstitials have been reported in GaAs grown by the horizontal Bridgman and liquid-encapsulated Czochralski methods, based on X-ray diffuse scattering⁷⁻⁹ and quasi-forbidden X-ray reflection intensity measurements.¹⁰ However, the atomic composition and microscopic structure of these defects cannot be unambiguously determined from these experiments.

Gallium arsenide grown by arsenic-rich molecular beam epitaxy at low temperature (LT GaAs) is a semi-insulating material with a host of potentially useful applications.¹¹ This material contains up to 1.5% excess As,¹² which is accommodated by high concentrations of point defects in UN-annealed samples, and arsenic precipitates plus somewhat lower concentrations of point defects in annealed samples. Concentrations of As antisites (As_{Ga}) up to 10^{20} cm^{-3} are observed in LT GaAs, as measured by electron paramagnetic resonance (EPR),¹³ near-infrared absorption (NIRA) and magnetic circular dichroism of absorption (MCDA),¹⁴ and scanning tunneling microscopy (STM).¹⁵ Concentrations of Ga vacancies (V_{Ga}) up to 10^{18} cm^{-3} are measured in LT GaAs by slow positron annihilation.¹⁶ Ion channeling experiments have been interpreted as providing evidence for large concentrations of As interstitials in LT GaAs.¹² However, it was later pointed out that the observed high concentration of atoms in the channel near the normal arsenic lattice sites could also be due to outward relaxation of the nearest neighbors of the As antisites.^{14,17}

Within certain well defined limits of the growth parameters for LT GaAs, a linear correlation between the neutral As_{Ga} concentration and the lattice dilation has been found.^{14,16} It was therefore proposed that As_{Ga} are the dominant defects which determine the lattice expansion for growth within this regime. Staab *et al.*¹⁷ used a self-consistent density-functional-based tight-binding method to study the lattice distortion induced by point defects

in As-rich GaAs, and concluded that only As_{Ga} are necessary to understand the observed lattice expansion in the regime where the linear correlation is observed, and that if concentrations of isolated As_i comparable to the measured concentrations of As_{Ga} were also present, the lattice expansion would be three times greater than is experimentally observed. However, Luysberg *et al.* have reported that when the As/Ga flux ratio is increased beyond a beam equivalent pressure (BEP) ratio of 20, there is a departure from the linear correlation between lattice dilation and antisite concentration.¹⁶ It was pointed out that other defects must be present to account for the deviation from stoichiometry and the lattice expansion at high As/Ga flux ratios.¹⁶

Nonequilibrium processes such as diffusion and compositional intermixing at interfaces can also be strongly affected by point defects that are present in high concentrations. Since the point defects which have been unambiguously documented as present in high concentrations in LT GaAs, As_{Ga} and V_{Ga} , occupy sites on the gallium sublattice, they cannot contribute directly to interdiffusion on the arsenic sublattice. However, substantial concentrations of arsenic interstitials may affect interdiffusion on the arsenic sublattice. For example, an experimental study showing a positive dependence of GaAsP/GaAs and GaAsSb/GaAs interdiffusion on arsenic pressure has indicated that a knockout mechanism involving arsenic interstitials is the dominant process for the As-P and As-Sb interdiffusion in the material studied.¹⁸

Similarly, annealing LT-GaAs δ -doped with Sb was found to produce substantially greater compositional intermixing than annealing conventional stoichiometric GaAs similarly δ -doped.¹⁹ This enhancement of As-Sb interdiffusion was attributed to an oversaturation of arsenic interstitials in the LT GaAs samples, resulting from the balance of arsenic interstitials with arsenic clusters and all the other excess-arsenic-containing defects in the material. The effective activation energy for As-Sb interdiffusion in LT GaAs deduced from this work, 0.6 ± 0.15 eV,¹⁹ is reasonably close to the migration energy of 0.5 eV for arsenic interstitials deduced from annealing experiments on defects produced by electron irradiation,¹ as well as to migration energies subsequently ascribed to arsenic interstitial defects produced in GaAs by other means. The concentration of arsenic interstitials required to produce sufficient oversaturation to eliminate completely any contribution of the interstitial formation energy to the activation energy for As-Sb intermixing measured in the LT GaAs sample was estimated to be roughly 10^{18} cm^{-3} , using Hurlé's thermodynamic analysis in conjunction with the experimental data.¹⁹

Theoretical attempts to obtain a picture of the microscopic structure and properties of the lowest energy arsenic interstitial configuration(s) began with the work of Baraff and Schlüter, who used density functional Green's function calculations to investigate the energies of reactions creating native defects with T_d symmetry in GaAs, including arsenic interstitials in the two tetrahe-

dral sites.²⁰ The effects of lattice relaxation were ignored. Baraff and Schlüter concluded that simple tetrahedral arsenic interstitials were less likely to occur than vacancy and antisite defects under all equilibrium conditions, although they could not rule out the possibility that other, more complicated interstitial configurations might have a lower energy.²⁰

Jansen and Sankey calculated the formation energies for unrelaxed native defects with tetrahedral symmetry in GaAs, including arsenic interstitials in tetrahedral sites, using a density-functional pseudopotential method with a basis set of pseudo-atomic orbitals and a single special \mathbf{k} -point in supercells containing about 32 atoms.²¹ In order to calculate the formation energies for individual defects instead of reaction energies for defect reactions which conserve the number of atoms of each species, they were required to choose a value for the arsenic chemical potential (or equivalently, for the gallium chemical potential). An arbitrary value was chosen, corresponding to the condition that the formation energies for neutral gallium vacancies and for neutral arsenic vacancies should be equal. Jansen and Sankey concluded that arsenic interstitials in tetrahedral sites should be less numerous than vacancies and antisites in GaAs under equilibrium conditions,²¹ in agreement with Baraff and Schlüter.

Zhang and Northrup used density functional theory (DFT) within the local density approximation (LDA) and supercells of about 32 atoms to calculate the formation energies for vacancies, antisites, and tetrahedral interstitials in GaAs as a function of arsenic chemical potential, over the physically allowable range of chemical potentials, from Ga-rich to As-rich.²² This physically allowable range is set by the heat of formation of bulk GaAs and by the requirement that the arsenic chemical potential may not exceed the chemical potential of bulk arsenic, since the material is in equilibrium with arsenic precipitates in the arsenic-rich limit. The atomic coordinates were allowed to relax in these calculations, within the constraints imposed by the tetrahedral symmetry. In agreement with the previous work, Zhang and Northrup found that antisites and/or vacancies should be more numerous than arsenic interstitials in tetrahedral sites under all equilibrium conditions.²²

Chadi used DFT-LDA calculations and 33-atom supercells to investigate many different types of bonding configurations for self-interstitials in GaAs, including various split interstitials, as well as hexagonal, two-fold coordinated, and tetrahedral interstitials, all fully relaxed within the constraints of the chosen symmetry.²³ He found that the lowest energy configuration for arsenic interstitials in the neutral or -1 charge state is a split interstitial consisting of two As atoms sharing an arsenic lattice site, displaced from this site in opposite directions along a $\langle 110 \rangle$ -like axis, while the lowest energy configuration for positively charged arsenic interstitials in the $+1$ or $+2$ charge state is a split interstitial consisting of an As atom and a Ga atom sharing a gallium lattice site, displaced from this site in opposite directions along

a $\langle 100 \rangle$ -like axis. Since we will be interested below primarily in arsenic interstitials in semi-insulating or n -type GaAs, we will use the notation As_i -As for the interstitial with two atoms sharing an arsenic site and aligned along a $\langle 110 \rangle$ -like axis, which should be the lowest energy interstitial configuration in semi-insulating or n -type material.

Chadi also showed that neutral arsenic interstitials, which have unpaired spins, are unstable relative to formation of a pair of $+1$ and -1 charged interstitials — *i.e.* arsenic interstitials form a negative- U system. This suggested that arsenic interstitials may not be observable in EPR experiments.²³ Chadi reported the relative energies for the most energetically favorable arsenic interstitial configurations in each of these charge states, including in each case a number of metastable configurations somewhat higher in energy than the lowest energy configurations, all of which were more complicated than the simple tetrahedral configurations.²³ However, since Chadi did not report absolute interstitial formation energies as a function of arsenic chemical potential, no comparison with the formation energies of defects involving a different number of excess arsenic atoms, such as arsenic antisites, was possible from this work.

Landman *et al.* investigated the relative formation energies of the point defects containing excess As, As_{Ga} , V_{Ga} , and the lowest energy As_i configuration in semi-insulating or n -type, As-rich GaAs, As_i -As,²⁴ using DFT-LDA-based calculations with the Harris-Foulkes functional and a basis of pseudo-atomic orbitals.^{25,26} They placed the defects in 64-atom supercells, and estimated summations in \mathbf{k} -space by using a single Chadi and Cohen special point.²⁷ Since Harris-Foulkes, pseudoatomic-orbital calculations do not give as accurate results for semiconductor heats of formation or for the relative energies of compound semiconductor and pure, metallic phases as fully self-consistent DFT-LDA calculations with a sufficiently large basis of plane waves, they did not use this method to calculate the arsenic chemical potential in the arsenic-rich limit. Instead, the relative formation energies of the tetrahedral As_i with arsenic nearest neighbors, As_{Ga} , and V_{Ga} in the arsenic-rich limit for the chemical potential were taken from information given by Zhang and Northrup,²² and the relative formation energy of As_i -As was determined by Landman *et al.*'s result that the neutral As_i -As is 4 eV lower in energy than the unrelaxed, neutral tetrahedral As_i with arsenic nearest neighbors. Since the tetrahedral interstitial was found to be unstable, relaxing to another configuration in Landman *et al.*'s calculation, they were obliged to compare their results for the ideal, unrelaxed tetrahedral interstitial to Zhang and Northrup's results for a tetrahedral interstitial which had been relaxed while constrained to keep its tetrahedral symmetry. This led to an additional uncertainty in the relative formation energies between zero and 0.8 eV.²⁴ However, Landman *et al.* concluded that the lowest energy split As_i may have a concentration approaching that of As_{Ga} for certain Fermi levels.²⁴

Since the theoretical investigations described above have been carried out over a long period of time, it has gradually become possible not only to include lattice relaxation and to investigate more complicated interstitial configurations, but also to do more accurate calculations, using larger unit cells and better sets of \mathbf{k} -points for the summations over \mathbf{k} -space. Pöykko *et al.* showed how sensitive calculated defect properties can be to the \mathbf{k} -space sampling method and supercell size in their investigation of the V_{As} - Si_{Ga} complex in GaAs.²⁸ They found that the use of the Γ point can produce misleading results even when supercells are 64-atoms in size, reinforcing the conclusions of Makov that the Γ point produces particularly slowly converging results with respect to cell size.²⁹ So it is essential to use a special point mesh in this type of calculation. Furthermore, Puska *et al.* concluded that cell sizes of 128 to 216 atoms are needed to properly assess the physical properties of the silicon vacancy in bulk silicon, because of the dispersion of energy levels and long range ionic relationships.³⁰

In this paper, we investigate the combined effects of cell size and \mathbf{k} -space sampling on the formation energy, charge state transitions, atomic relaxations, and characterization of localized defect states for arsenic self-interstitials in GaAs. Because of the more ionic nature of the material and the complicated split interstitial defect structure, comparison of these results for interstitials in GaAs to the previous results for vacancies in silicon³⁰ can enhance our understanding of the range of behavior for different defects in different materials. We compare the formation energy of the lowest energy arsenic interstitial in n -type or semi-insulating GaAs, As_i -As, with the formation energies of As_{Ga} and V_{Ga} at the arsenic-rich end of the range of physically allowed chemical potentials, all calculated by state-of-the-art DFT pseudopotential³¹ calculations, using the larger supercells and sets of special \mathbf{k} -points which we have determined to be necessary. We conclude our study by discussing the relative concentrations of these defects in equilibrium in As-rich, n -type or semi-insulating GaAs at growth temperatures, and reporting the computed charge transition levels and expected electrical behavior of As_i -As as a function of Fermi level.

II. COMPUTATIONAL METHOD

We have used the molecular dynamics code developed at the Fritz Haber Institut (FHIMD)³¹ for this investigation, using density-functional theory (DFT)³² within the local density approximation (LDA), with the Ceperley-Alder³³ form for the exchange and correlation potentials as parameterized by Perdew and Zunger.³⁴ The core electrons are treated in the frozen-core approximation and the ion cores are replaced by fully-separable³⁵ norm-conserving pseudopotentials.³⁶ Plane waves are included up to the energy cutoff of 10 Ry. The atoms are allowed to relax until the force components are

less than 5×10^{-4} hartrees per bohr radius and the zero temperature formation energies change by less than 5×10^{-6} hartrees per step for at least 100 steps.

To evaluate the defect formation energy, we used the formalism of Zhang and Northrup,²² which gives for the formation energy in the As-rich limit at zero temperature

$$\begin{aligned} \Delta E_f = & E(N_{\text{Ga}}, N_{\text{As}}, q) - N_{\text{Ga}}\mu_{\text{GaAs}} \\ & - (N_{\text{As}} - N_{\text{Ga}})\mu_{\text{As(bulk)}} + q\epsilon_F. \end{aligned} \quad (1)$$

Here q electrons have been transferred to a reservoir at the Fermi energy ϵ_F in order to produce a defect in the desired charge state. $E(N_{\text{Ga}}, N_{\text{As}}, q)$ is the zero-temperature total energy produced by the *ab initio* code for a supercell containing the desired defect, the chemical potential μ_{GaAs} is the energy per atomic pair of bulk GaAs, and the arsenic chemical potential in the As-rich limit, $\mu_{\text{As(bulk)}}$, is the energy per atom of pure bulk As computed using the same *ab initio* code and pseudopotentials. N_{Ga} and N_{As} are the numbers of atoms of each species in the supercell containing the defect. We will discuss the effect of temperature, which can be important for defect concentrations, in Section III.

Because the zero of the energy levels floats freely,³⁷ results from different DFT supercell calculations must be aligned in order to obtain the correct charge transition levels. We apply the procedure outlined by Kohan *et al.*³⁸ in which we first compute the difference between the electrical potential in the supercell with the neutral defect and the electrical potential for the corresponding bulk crystal supercell, averaged over parallel planes, as a function of position along a line normal to the planes. Far from the defect within the supercell, this difference becomes a constant. In order to make the potential far from the neutral defect equal to the corresponding potential in the bulk cell, a uniform shift is applied to the potential and the energy levels, yielding the proper alignment of the energy levels of the defect with the energy levels of ideal bulk crystal supercell. The same shift is applied for all charge states of a given defect.

A well-known shortcoming of the LDA is that it underestimates the band gaps of materials. The typical method for dealing with this problem is to simply shift the conduction band states up uniformly by the amount needed to reproduce the experimental gap, using the so-called ‘scissors operator’.³⁹ More recently, an analytically-based model justifying the rigid shifting upward of all conduction band states by a scissors-type correction has been shown to produce good results for a large number of semiconductors.⁴⁰ Since the LDA can produce similarly large errors in the energies of the deep defect states, it is also important to correct for these errors when determining where the charge transition levels corresponding to deep defect states lie in the experimental gap. Unfortunately, a full GW calculation,^{41–45} which would correct these errors, is not currently possible for the large supercells needed for studies of defects. Therefore, we apply the same upward shift to the defect states with predominantly conduction band character as is applied to the

conduction band states themselves, while leaving the defect states with predominantly valence band character fixed relative to the valence band edge.

III. RESULTS AND DISCUSSION

A. Defect formation energies, charge transition levels, and localized defect states

We used cubic supercells with dimensions of both two and three times the computationally determined bulk lattice constant, corresponding to bulk cells of 64 and 216 atoms, along with three different Brillouin zone (BZ) sampling schemes to examine the effects cell size and sampling scheme have on the formation energies and transition levels for the $\text{As}_i\text{-As}$. In order to investigate the most efficient choice of \mathbf{k} -points to obtain good results, we have used a 1^3 Monkhorst-Pack (MP) mesh,⁴⁶ a 2^3 MP mesh, and the Γ and L points, which was recommended as a good minimal set of \mathbf{k} -points for cubic supercells with no particular symmetry within the supercell,²⁹ and which has subsequently been used in defect calculations, *e.g.* to study the structures associated with dopants in highly n -doped Si.⁴⁷ Calculations comparing different summation schemes for vacancies in Si show that use of the $\Gamma + L$ points produces a reasonably well-converged formation energy in a 64-atom supercell.³⁰

This earlier work on the vacancy in silicon has shown that the neutral vacancy formation energy computed with different \mathbf{k} -space sampling schemes converges at different rates with respect to supercell size.³⁰ However, an acceptably converged value for the neutral vacancy formation energy can be attained more easily than an acceptably converged description of the charge transition levels and the atomic relaxations and defect symmetry for different charge states.³⁰

To augment our understanding of the effects of cell size and sampling scheme, we computed the formation energies of the different charge states for the fully relaxed split interstitial $\text{As}_i\text{-As}$ in GaAs. Charge was balanced by a uniform background to avoid long range Coulomb interactions between the supercells.

Table I lists the formation energies we obtained for all the excess-arsenic-containing elementary point defects in the arsenic-rich limit, with GaAs in equilibrium with bulk arsenic, including complete results for the various \mathbf{k} -space sums for $\text{As}_i\text{-As}$. For comparison, the formation energies of the unrelaxed, ideal tetrahedral As interstitials with As neighbors (As_{i1}) and with Ga neighbors (As_{i2}) are also shown. These tetrahedral interstitials are unstable, and will relax to other configurations if allowed to break their tetrahedral symmetry.

Table I displays formation energies evaluated for the Fermi level at the valence band maximum (VBM), and also for the Fermi level pinned at the calculated position of the (+1/0) charge state transition of the As_{Ga} , which is at VBM+0.54 eV for the 2^3 MP mesh and VBM+0.45 eV

TABLE I. Formation energies for excess-arsenic-containing defects computed in the As-rich limit. These were calculated with supercells corresponding to the bulk 216 atom cell. The values in the last column are computed with the Fermi level pinned at the calculated (+1/0) transition level of the As antisite defect.

Defect	k -space sum	Charge state	Formation energy (eV) ϵ_F at VBM	Formation energy (eV) semi-insulating ϵ_F
As _{Ga}	MP 2^3	+2	0.9	2.0
As _{Ga}	MP 2^3	+1	1.3	1.8
As _{Ga}	MP 2^3	0	1.8	1.8
As _{Ga}	MP 1^3	+2	0.9	1.8
As _{Ga}	MP 1^3	+1	1.1	1.6
As _{Ga}	MP 1^3	0	1.6	1.6
As _{i1}	MP 2^3	0	6.9	6.9
As _{i2}	MP 2^3	0	6.2	6.2
As _i -As	MP 2^3	+1	3.5	4.1
As _i -As	MP 2^3	0	3.8	3.8
As _i -As	MP 2^3	-1	4.4	3.8
As _i -As	MP 1^3	+1	3.4	3.8
As _i -As	MP 1^3	0	3.7	3.7
As _i -As	MP 1^3	-1	4.1	3.7
As _i -As	$\Gamma + L$	+1	3.6	
As _i -As	$\Gamma + L$	0	3.6	
As _i -As	$\Gamma + L$	-1	4.1	
V _{Ga}	MP 2^3	0	2.9	2.9
V _{Ga}	MP 2^3	-1	3.0	2.5
V _{Ga}	MP 2^3	-2	3.1	2.1
V _{Ga}	MP 2^3	-3	3.4	1.8

for the 1^3 MP mesh. This choice of Fermi level was based on the experimental finding that there can be high concentrations of As_{Ga} in As-rich GaAs, and that these high concentrations of As_{Ga} can pin the Fermi energy near this transition level. Using either choice of Fermi level as a reference, the formation energies and equilibrium concentrations of the defects can be determined as a function of Fermi energy (or doping level).

In Fig. 1, we present the results of the formation energy calculations for As_i-As in which both cell size and k -space sampling methods have been varied. This figure shows the formation energy for the As_i-As in its preferred charge state. For Fermi levels in the range where the neutral As_i-As is preferred, the formation energy is independent of Fermi level. If the Fermi level is decreased past the (0/+1) charge transition level, so that the +1 charge state is preferred, the formation energy vs. Fermi level curve has a slope of +1, as can be seen from Eq. (1), and if the Fermi level is increased past the (0/-1) charge transition level, so that the -1 charge state is preferred, the formation energy vs. Fermi level curve has a slope of -1.

The most obvious feature in Fig. 1 is the wider variation in the energies computed using the smaller supercell. Convergence with cell size is also visibly slower when using the 1^3 MP mesh or the $\Gamma + L$ points, which use a

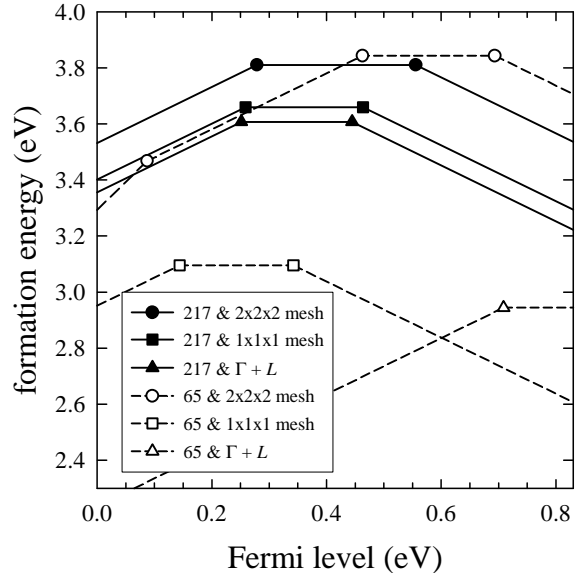


FIG. 1. Defect formation energies for the As split interstitial computed in the As-rich limit. Comparisons are presented for different k -space sums and two supercell sizes. Dashed lines are used for cells containing 65 atoms, and solid lines for 217 atom cells. Transition levels between the different charge states are marked with circles for the 2^3 MP mesh, squares for the 1^3 MP mesh, and triangles for the $\Gamma + L$ k -space sum.

less finely spaced set of k -points than the 2^3 MP mesh to cover the Brillouin zone. It is clear that the 217 atom cell with the 2^3 MP mesh is well converged. We see that the two less finely spaced sampling schemes produce somewhat converged results in the 217 atom cell, as does the 2^3 MP mesh in the 65 atom cell. In agreement with previous results for the vacancy in bulk Si,³⁰ we find that different sampling schemes can be used to produce either an attraction between defects (*i.e.* a lowering of energy in the smaller supercell), as in the 1^3 MP or the $\Gamma + L$ cases, or a charge-state dependent repulsion or attraction between defects, as in the 2^3 MP case.

When comparing the results for the 65-atom and the 217-atom cells, using the 2^3 MP mesh, we see that the charge transition levels converge less rapidly than the neutral defect formation energy with increasing cell size, due to long-range interactions of the electrons in the localized defect state with the charged defects in neighboring cells. The neutral As_i-As formation energy changes by less than 0.1 eV when the cell size is reduced from 217 to 65 atoms, while the charge transition levels move by about 0.4 eV, when using the 2^3 MP mesh. This trend is not seen in the less-well-converged results obtained using the 1^3 MP mesh or the $\Gamma + L$ points, where the neutral As_i-As formation energies move by 0.5 to 0.6 eV when the cell size is reduced from 217 to 65 atoms, perhaps due to interactions of the deep defect level with the band edges.

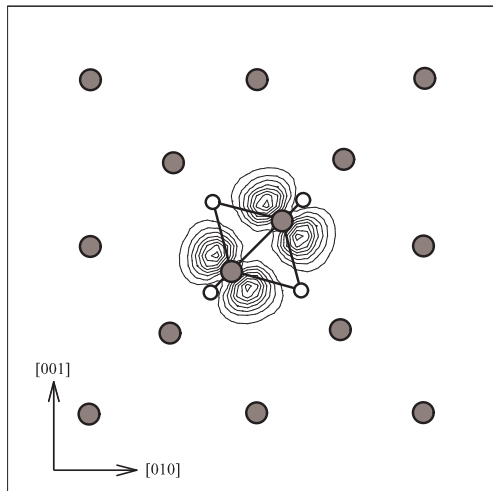


FIG. 2. This contour plot shows levels of constant charge density for the localized defect state of the neutral $\text{As}_i\text{-As}$ in the 217 atom supercell, evaluated in the plane containing the two defect As atoms, which is 0.48\AA above the As lattice site associated with the defect. The dark circles represent the positions of the As atoms, including the defect atoms and the As atoms of the original lattice plane. The light circles show the locations of the neighboring Ga atoms projected onto the plane.

In the neutral charge state, the topmost filled electronic level is half filled. This level corresponds to a localized state centered on the split interstitial oriented along a $\langle 110 \rangle$ -like direction. In Fig. 2, the charge density associated with this defect state is shown in a plane parallel to an arsenic lattice plane, but slightly above this plane, so that it includes the two arsenic atoms of the split interstitial, which have relaxed slightly away from the ideal lattice site. This plot clearly shows that the defect state is localized in p -like orbitals which appear to be forming a π antibonding state, as evident from the node in the charge density midway between the two As atoms forming the split interstitial. This result is corroborated by an examination of the characterization of the state, using the 217-atom cell and the 2^3 MP mesh, which shows that in contrast to the very extended character of the bulk-like states, 20% of the defect state is localized in the p_y and p_z orbitals of the two As atoms of the neutral defect. Since the charge density in this defect state points roughly along the direction of the As-Ga bonds between the defect As atoms and the two Ga atoms bonded to both of these As atoms, we note that this state makes a bonding contribution to these As-Ga interactions as well as making an antibonding contribution to the interaction between the As atoms of the defect.

The characterization of the deep defect state in the 217-atom supercell is not very sensitive to the \mathbf{k} -space sampling method used. For example, 20% of the state

is also found to be localized in the p_y and p_z orbitals of the two As atoms of the neutral defect when the $\Gamma + L$ sampling is used.

In smaller supercells, the defect state interacts with its images and becomes less localized. One way to observe this is to examine the variation in energy of the defect state across \mathbf{k} -space, *i.e.* the dispersion of the state. We characterize this variation by computing the difference between the highest and lowest energy obtained from a \mathbf{k} -space survey along the Δ , Σ , Λ , and T lines in the cubic Brillouin zone. The dispersion measured in this way is 0.1 eV in the 217 atom supercell, and 0.5 eV in the 65 atom cell. This interaction of the defects in neighboring supercells contributes to the variation in the positions of the charge transition levels between the different cell sizes and sampling schemes, noted above, and supports the conclusion that the larger 217 atom supercell should be used for accuracy in describing the charge transition levels and deep defect states.

B. Defect atomic structure and relaxation

The detailed structure of the atomic positions is also expected to be dependent on the cell size and \mathbf{k} -space sampling approach. However, in contrast to the behavior observed for the vacancy in silicon,³⁰ where the defect symmetry and atomic relaxations are very sensitive to the supercell size and \mathbf{k} -space sampling, we find that the atomic structure of the $\text{As}_i\text{-As}$ defect is remarkably similar for the 65-atom and 217-atom supercells, and also depends little on the \mathbf{k} -space sampling approach. In Fig. 3 we show the structure of the neutral split interstitial oriented along the $\langle 011 \rangle$ direction, viewed from the $[100]$ direction. The two Ga atoms labeled Ga(1) and Ga(3) are bonded to both As atoms of the defect, while those labeled Ga(2) and Ga(4) are bonded to only one of the defect atoms. The structure exhibits C_{2v} symmetry in all charge states and returns to this symmetry when the atomic coordinates are perturbed from their equilibrium positions and allowed to relax.

Although the local lattice expansion introduced by the additional atom of the interstitial might be expected to converge slowly with supercell size, we find that reasonable convergence is more easily reached for the atomic positions than for the electronic properties discussed in the previous section. The As-As and As-Ga distances found in the 65 atom supercell differ by less than 0.01\AA from those found in the 217 atom supercell, using the 2^3 MP mesh. The distance between the two As atoms of the $\text{As}_i\text{-As}$ defect is 2.39\AA . (For comparison, the GaAs bulk nearest neighbor distance in this calculation is 2.41\AA .) The distance between Ga(1) or Ga(3) and either of the As atoms of the defect is 2.60\AA . The distance between Ga(2) or Ga(4) and the nearest As of the split interstitial is 2.32\AA .

The two different supercell sizes produce slightly different results in the position of the center of mass of

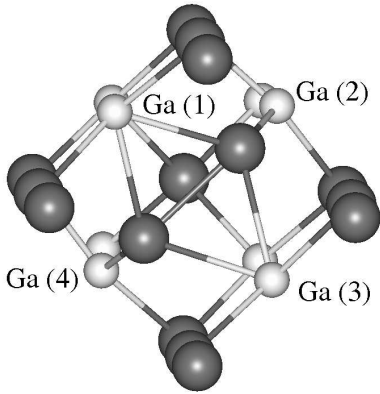


FIG. 3. The neutral $\text{As}_i\text{-As}$ defect from the 217-atom supercell is shown (viewed from a direction slightly displaced from the $[100]$ direction) with larger dark spheres representing the As atoms and smaller light spheres representing the Ga atoms.

the two As atoms of the split interstitial. The center of mass of the pair of As atoms is shifted away from the bulk lattice site by 0.48 \AA in the $[100]$ direction toward the plane containing Ga(1) and Ga(3) in the case of the 217 atom supercell, using the 2^3 MP mesh. This shift is 0.50 \AA in the smaller supercell. Since the nearest neighbor distances are very similar in the two supercells, this difference is accomplished through variation of bond angles. The angle between the bonds from one of the As atoms to the Ga(1) and Ga(3) atoms is 107.7° in the small supercell and 106.8° in the large supercell.

We find that the atomic structure of the $\text{As}_i\text{-As}$ defect depends very little on the \mathbf{k} -space summation method, as can be shown by examining the bond lengths between the As atoms of the defect and between those As atoms and the four neighboring Ga atoms in the 217 atom supercell. For the neutral $\text{As}_i\text{-As}$ defect, these bond lengths change by less than 0.1% when the summation method is changed.

For the $+1$ charge state of the defect, we find a small but perceptible dependence of the bond lengths on the \mathbf{k} -space summation method. The As-As distance obtained using the 2^3 MP mesh is about 1% smaller than that obtained using the $\Gamma + L$ sampling. The bond between either of the As atoms and the Ga(1) or Ga(3) atom is about 1% longer when using the 2^3 MP mesh than when using the $\Gamma + L$ summation method. The distance between the Ga(2) or Ga(4) atom and the nearest As atom of the split interstitial is about 0.5% longer for the 2^3 MP mesh calculation than for the $\Gamma + L$ calculation.

There is a similar but weak effect (under 0.5%) in the defect bond lengths observed in the -1 state, with the roles of the 2^3 MP mesh and the $\Gamma + L$ points reversed — *i.e.* the 2^3 MP mesh now gives a larger As-As distance and smaller As-Ga distances. The 1^3 MP mesh produces results between those of the other two \mathbf{k} -space summation methods.

The effect of these small variations in bond lengths is to reduce the changes in bond length seen in the 2^3 MP mesh calculations when the defect becomes charged, if one of the other \mathbf{k} -space sampling methods is used instead. In particular, the $\Gamma + L$ sampling is observed to produce a somewhat smaller dependence of these bond lengths on charge state. This dependence of bond lengths on the charge state of the defect is seen below to result from the changes in occupation of the deep defect state when the charge state is changed, and from the bonding or antibonding character of this state for particular bonds.

Focusing on results for the 217 atom cell with the 2^3 MP mesh, we observe that the distance between the atoms of the defect has a significant dependence on the charge state of the system. The As-As bond expands to 2.47 \AA (about 3.5% compared to the neutral state bond length), when the system is allowed to relax in the -1 charge state. This can be easily understood, since the antibonding defect state on the two As atoms is doubly occupied and can cause a stronger repulsive contribution to the interaction between these two atoms for the -1 charge state of the defect, while it is only singly occupied for the neutral state of the defect.

When the system is allowed to relax in the $+1$ state the As-As bond shrinks to 2.31 \AA , a contraction of about 3%. This can also be easily understood, since the antibonding defect state on the two As atoms of the defect is completely unoccupied for the $+1$ charge state, so it no longer makes a repulsive contribution to the interaction between the two As atoms. The bond length between Ga(1) or Ga(3) and either As atom of the defect is 3.5% longer and the bond length between Ga(2) or Ga(4) and the nearest defect As atom is 1.9% longer in the $+1$ state than in the neutral state. Since the deep defect state acts as a bonding state for the As-Ga bonds between the defect As atoms and Ga(1) and Ga(3), as discussed above in Section III A, it is easy to understand why these bonds are longer in the $+1$ state, when the defect state is fully unoccupied and can no longer contribute to the strength of these bonds.

We note that because of the contribution of the defect state to the As-Ga bonds between the defect As atoms and Ga(1) and Ga(3), these two Ga atoms move significantly when the charge state is changed, changing the occupation of the defect state. These Ga atoms are about 4% closer to each other in the -1 state and about 5.5% farther apart in the $+1$ state than in the neutral state. The other two Ga atoms, each bonded to only one defect As atom, do not move in response to the change in charge state.

In performing these calculations, we fixed the lattice constant at the value determined through minimization of the energy of the bulk crystal. While the ideal calculation should include a full lattice constant determination with each change of defect configuration, for simplicity we did not perform this relaxation. This may be deemed a reasonable choice in light of evidence presented by Puska,

*et al.*³⁰ for *ab initio* supercell calculations in the LDA, using supercells of sizes comparable to ours, in which vacancies in bulk Si are found to alter the lattice constant by around 0.2%, while artificially introduced distortions in the lattice constant of up to 1% are seen not to affect their reported results significantly.

C. Relative defect concentrations in equilibrium

We now compare our well-converged results for the formation energies of the elementary excess-arsenic-containing point defects, As_{Ga} , V_{Ga} , and $\text{As}_i\text{-As}$ (the most favorable As_i configuration in semi-insulating or *n*-type GaAs), computed using the large supercell and the 2^3 MP mesh. These formation energies in the As-rich limit, corresponding to GaAs in equilibrium with bulk arsenic, are presented as a function of Fermi energy in Fig. 4. The formation energies for two specific choices of Fermi energy have also been listed in Table I in Section III A.

In Fig. 4, we can see that the V_{Ga} and As_{Ga} defects possess significantly lower formation energies than the $\text{As}_i\text{-As}$ for all Fermi energies. For example, the formation energy for As_{Ga} is seen to be at least 2 eV lower than the formation energy for $\text{As}_i\text{-As}$ for all Fermi energies. Small uncertainties in the formation energy should not alter this strong qualitative ordering of the formation energies or the prediction based on this ordering that equilibrium concentrations of $\text{As}_i\text{-As}$ should be significantly lower than equilibrium concentrations of As_{Ga} , as discussed below.

To estimate equilibrium concentrations of the excess-arsenic-containing defects we begin with the usual expression

$$C = N e^{-\Delta E_f/k_B T} e^{S_f/k_B} e^{-P\Delta V_f/k_B T}, \quad (2)$$

where N is the number of sites at which the defect can form in the crystal per unit volume, ΔE_f is the total energy of formation of the defect, k_B is the Boltzmann constant, and T is the temperature. The formation entropy of the defect is S_f , P is the pressure, and ΔV_f is the change in the crystal volume associated with the defect formation.

We note that the defect formation energy ΔE_f for charged defects, as given by the formula in Eq. (1), has an explicit dependence on the Fermi energy, in addition to its dependence on the calculated energies for defect formation at zero Fermi energy. Therefore we must compute the Fermi energy self-consistently, in order to determine the native defect concentrations present in a particular sample. If any electrically active impurities or dopants are present in the material, the concentrations of these impurities or dopants in all charge states must also be taken into account. We must set up the charge balance equation, requiring that the free electron and hole concentrations (which also depend on the Fermi level) must

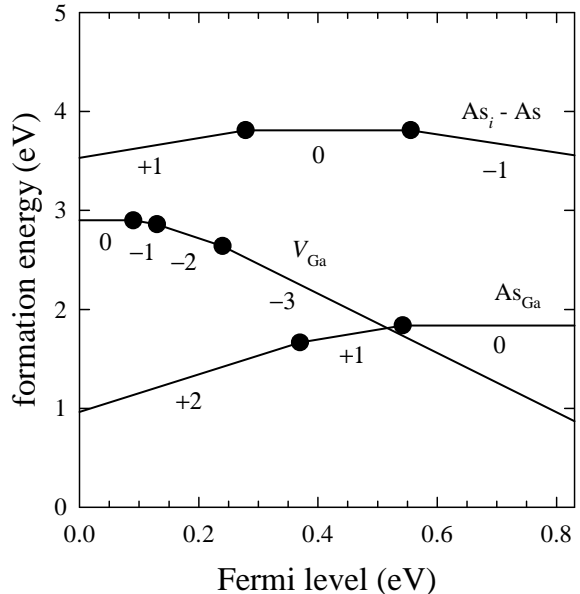


FIG. 4. Defect formation energies for selected defects over the calculated band gap in the As-rich limit. Zero Fermi level corresponds to the valence band maximum.

cancel out any net charge resulting from the concentrations of all positively and negatively charged defects and impurities. This equation can then be solved to determine the Fermi level. Once the Fermi level is known, it may be used to determine the formation energies and the resulting equilibrium concentrations of all the defects present.

If the defect formation energy E_f for the most energetically favorable charge state of $\text{As}_i\text{-As}$ in a particular sample is within $k_B T$ of the formation energy of the most favorable charge state of As_{Ga} , we may expect that the equilibrium concentrations of these two defects are comparable, assuming that the effects of the entropy of formation S_f and the change in the crystal volume ΔV_f associated with the defect formation can be neglected. We will now concentrate on the relative defect concentrations at 1500 K (near the melting point of GaAs), since defects with a higher formation energy such as $\text{As}_i\text{-As}$ have their greatest chance to attain equilibrium concentrations comparable to those of more energetically favorable defects at high temperature. We will estimate the effective corrections to the formation energy which occur at this temperature due to the entropy of formation and change in volume associated with the defects.

First, to estimate the effect of the change in volume, we let P be atmospheric pressure and overestimate ΔV_f to be the volume per bulk atom in the cell, which gives an effective correction to the defect formation energy $P\Delta V_f$ of 9×10^{-5} eV. We may safely neglect this correction.

Previous calculations⁴⁸ on defects in Si found that the

formation entropy S_f is dominated by vibrational contributions, and that the formation entropies are $6k_B$ and $5k_B$ for the self-interstitial and the vacancy, respectively. We note that the self-interstitial in silicon is a $\langle 110 \rangle$ split interstitial with the same basic structure as $\text{As}_i\text{-As}$ in GaAs. Therefore, in analogy to the results for defects in silicon,⁴⁸ we may assume that it is unlikely for the split interstitial $\text{As}_i\text{-As}$ to have a very different formation entropy when compared to defects such as As_{Ga} , which only contain atoms occupying lattice sites. If we let $S_f = 10k_B$ (an overestimate) for $\text{As}_i\text{-As}$, this gives rise to an effective reduction of the defect formation energy by $S_f T$, or 1.3 eV at 1500 K. Even if we apply no reduction to the As_{Ga} formation energy due to entropy, this still leaves the effective formation energy about 0.7 eV higher for $\text{As}_i\text{-As}$ than for As_{Ga} , producing equilibrium concentrations of $\text{As}_i\text{-As}$ which are about 0.4% those of As_{Ga} at 1500 K.

We conclude that even using this extremely liberal estimate for the formation entropy of $\text{As}_i\text{-As}$ and ignoring the formation entropy of As_{Ga} cannot lead to an $\text{As}_i\text{-As}$ concentration approaching that of the antisites in thermal equilibrium.

D. Defect electrical behavior

Although the placement of the calculated charge transition levels in the experimental gap has an uncertainty far exceeding 0.1 eV due to the shortcomings of the LDA in calculating the gap, as discussed in Section II, our as-calculated band gap and charge transition levels are reported here to 0.1 eV (or 0.01 eV, for the closely spaced V_{Ga} levels), for the convenience of the reader who prefers not to read them off the picture in Fig. 4. For the As_{Ga} , the $(+2/+1)$ transition level appears at 0.4 eV above the VBM, and the $(+1/0)$ level is at $E_{\text{VBM}} + 0.5$ eV. For the $\text{As}_i\text{-As}$, the $(+1/0)$ transition is at $E_{\text{VBM}} + 0.3$ eV, and the $(0/-1)$ transition is at $E_{\text{VBM}} + 0.5$ eV. The levels for the V_{Ga} defect are at 0.09 eV, 0.13 eV, and 0.2 eV above the VBM for the $(0/-1)$, $(-1/-2)$, and $(-2/-3)$ transitions, respectively. The calculated band gap of 0.8 eV is underestimated by 0.7 eV compared to the experimental zero-temperature gap of 1.5 eV.

As discussed previously in Section II, we can get a rough estimate of where the charge transition levels fall within the experimental gap by shifting the conduction band derived states (including the deep defect states with primarily conduction band character) by the amount needed to correct the gap, while leaving the defect states with predominantly valence band character fixed relative to the valence band edge. Since the acceptor levels of the V_{Ga} are derived from the dangling bonds on the arsenic neighbors of the vacancy, which require three extra electrons to fill them, they should have the predominantly valence band character of anion dangling bond states. In Section III A, the deep defect state of the $\text{As}_i\text{-As}$ was shown to have predominantly arsenic p -type character,

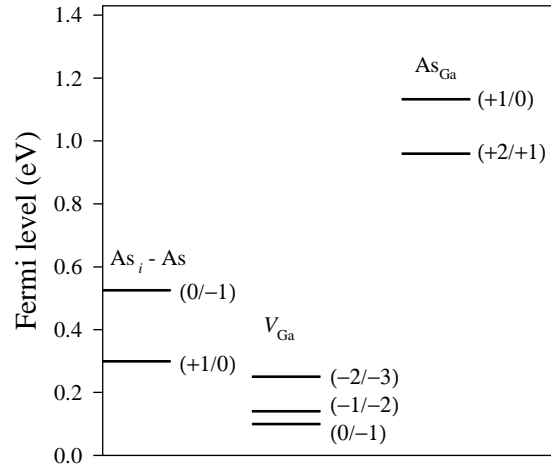


FIG. 5. Transition levels computed with a rigid shift applied to the conduction band and conduction band derived states to correct the LDA band gap underestimate.

similar to the character of the valence band edge states. However, the As_{Ga} double donor defect state derives from an antibonding state of predominantly conduction band character, which has been lowered in energy due to the replacement of the original anion-cation bonds of the ideal crystal by anion-anion bonds between the antisite and its nearest neighbors. This donor state is occupied by the two extra electrons contributed by the arsenic atom that has been substituted for a gallium atom, which cannot be accommodated in the bonding states of the valence band.

We conclude that the charge transition levels of the V_{Ga} and the $\text{As}_i\text{-As}$ should remain fixed relative to the valence band edge, while the donor levels of As_{Ga} , which possess a conduction band character, should be shifted up together with the conduction band states. In Fig. 5, we show the charge transition levels for these defects corrected by the above procedure, using the room temperature gap of 1.4 eV. The transition levels of As_{Ga} are shifted to 1.0 eV and 1.1 eV, in fortuitously good agreement with the MCDA results identified with this defect in LT GaAs,^{14,49} although the transitions are both about 0.4 eV higher than those associated with As_{Ga} in melt-grown GaAs.⁵⁰

IV. SUMMARY

In this work we have shown that larger supercells and a better \mathbf{k} -space sampling than have been used in a large number of previous DFT defect calculations are required to give accurate results for the formation energies, charge transition levels, defect state properties, and atomic structure and relaxation for the arsenic split

interstitial in GaAs. In particular, we find that 217-atom supercells are necessary to get good results for the charge transition levels and the dispersion of the deep defect state, even though the arrangement of atoms in the structure is well converged in a 65-atom cell, particularly if one uses the finely spaced 2^3 MP \mathbf{k} -space mesh.

We have calculated formation energies for As split interstitials, Ga vacancies, and As antisites in As-rich GaAs using the larger supercells and better \mathbf{k} -point sampling which we have determined to be necessary. Using these results, we find that the equilibrium concentrations of arsenic interstitials will be substantially lower than equilibrium concentrations of arsenic antisites in As-rich, n -type

or semi-insulating GaAs.

ACKNOWLEDGMENTS

This work was supported in part by AFOSR Grants No. F49620-96-1-0167 and No. F49620-97-1-0472, and by grants of time on the Cray T3e computers at the DOD HPC Centers at NAVO and ERDC and at the NPACI San Diego and University of Texas Supercomputing Centers, and on the NPACI AMD cluster at the University of Michigan. We also thank G. Schwartz and M. Bockstedte for highly useful conversations.

* joseph.schick@villanova.edu

¹ J. C. Bourgoin, H. J. von Bardeleben, and D. Stievenard, *J. Appl. Phys.* **64**, R65 (1988).
² D. T. J. Hurle, *J. Appl. Phys.* **85**, 6957 (1999).
³ D. T. J. Hurle, *Materials Science Forum* **196-201**, 179 (1995).
⁴ D. T. J. Hurle, *Non-Stoichiometry in Semiconductors* (Elsevier, New York, 1992), p. 47.
⁵ O. Oda, *Semiconductor Science and Technology* **7**, A215 (1992).
⁶ V. T. Bublik, *Sov. Phys. Crystallog.* **18**, 218 (1973).
⁷ L. Charniy and V. Bublik, *J. Crystal Growth* **135**, 302 (1994).
⁸ L. A. Charniy, A. N. Morozov, V. T. Bublik, K. D. Scherbachev, I. V. Stepanтова, and V. M. Kaganer, *J. Crystal Growth* **118**, 163 (1992).
⁹ L. A. Charniy, A. N. Morozov, K. D. Scherbachov, V. T. Bublik, and I. V. Stepanтова, *J. Crystal Growth* **116**, 369 (1992).
¹⁰ I. Fujimoto, *Materials Science and Engineering* **B14**, 426 (1992).
¹¹ D. D. Nolte, *J. Appl. Phys.* **85**, 6259 (1999).
¹² K. M. Yu, M. Kaminska, and Z. Liliental-Weber, *J. Appl. Phys.* **72**, 2850 (1992).
¹³ M. Kaminska, Z. Liliental-Weber, E. R. Weber, T. George, J. B. Kortright, F. W. Smith, B.-Y. Tsaur, and A. R. Calawa, *Appl. Phys. Lett.* **54**, 1881 (1989).
¹⁴ X. Liu, J. Nishio, E. R. Weber, Z. Liliental-Weber, and W. Walukiewicz, *Appl. Phys. Lett.* **67**, 279 (1995).
¹⁵ R. M. Feenstra, J. M. Woodall, and G. D. Pettit, *Phys. Rev. Lett.* **71**, 1176 (1993).
¹⁶ M. Luysberg, H. Sohn, A. Prasad, P. Specht, Z. Liliental-Weber, E. R. Weber, J. Gebauer, and R. Krause-Rehberg, *J. Appl. Phys.* **83**, 561 (1998).
¹⁷ T. E. M. Staab, R. M. Nieminen, J. Gebauer, R. Krause-Rehberg, M. Luysberg, M. Haugk, and T. Frauenheim, *Phys. Rev. Lett.* **87**, 045504 (2001).
¹⁸ M. Schultz, U. Egger, R. Scholz, O. Breitenstein, U. Gösele, and T. Y. Tan, *J. Appl. Phys.* **83**, 5295 (1998).
¹⁹ V. V. Chaldyshev, N. A. Bert, Y. G. Musikhin, A. A. Suvorova, V. V. Preobrazhenskii, M. A. Putyato, B. R. Semagin, P. Werner, and U. Gösele, *Appl. Phys. Lett.* **79**, 1294 (2001).
²⁰ G. A. Baraff and M. Schlüter, *Phys. Rev. Lett.* **55**, 1327 (1985).

²¹ R. W. Jansen and O. F. Sankey, *Phys. Rev. B* **39**, 3192 (1989).
²² S. B. Zhang and J. E. Northrup, *Phys. Rev. Lett.* **67**, 2339 (1991).
²³ D. J. Chadi, *Phys. Rev. B* **46**, 9400 (1992).
²⁴ J. I. Landman, C. G. Morgan, J. T. Schick, P. Papoulias, and A. Kumar, *Phys. Rev. B* **55**, 15581 (1997).
²⁵ O. F. Sankey and D. J. Niklewski, *Phys. Rev. B* **40**, 3979 (1989).
²⁶ M.-H. Tsai, O. F. Sankey, and J. D. Dow, *Phys. Rev. B* **46**, 10464 (1992).
²⁷ D. J. Chadi and M. L. Cohen, *Phys. Rev. B* **8**, 5747 (1973).
²⁸ S. Pöykkö, M. J. Puska, M. Alatalo, and R. M. Nieminen, *Phys. Rev. B* **54**, 7909 (1996).
²⁹ G. Makov, R. Shah, and M. C. Payne, *Phys. Rev. B* **53**, 15513 (1996).
³⁰ M. J. Puska, S. Pöykkö, M. Pesola, and R. M. Nieminen, *Phys. Rev. B* **58**, 1318 (1998).
³¹ M. Bockstedte, A. Kley, J. Neugebauer, and M. Scheffler, *Comput. Phys. Commun.* **107**, 187 (1997).
³² P. Hohenberg and W. Kohn, *Phys. Rev.* **136**, B864 (1964).
³³ D. M. Ceperley and G. J. Alder, *Phys. Rev. Lett.* **45**, 566 (1980).
³⁴ J. Perdew and A. Zunger, *Phys. Rev. B* **23**, 5048 (1981).
³⁵ L. Kleinman and D. M. Bylander, *Phys. Rev. Lett.* **48**, 1425 (1982).
³⁶ D. R. Hamann, *Phys. Rev. B* **40**, 2980 (1989).
³⁷ L. Kleinman, *Phys. Rev. B* **24**, 7412 (1981).
³⁸ A. F. Kohan, G. Ceder, D. Morgan, and C. G. V. de Walle, *Phys. Rev. B* **61**, 15019 (2000).
³⁹ G. A. Baraff and M. Schlüter, *Phys. Rev. B* **30**, 1853 (1984).
⁴⁰ K. A. Johnson and N. W. Ashcroft, *Phys. Rev. B* **58**, 15548 (1998).
⁴¹ L. Hedin, *Phys. Rev.* **139**, A796 (1965).
⁴² L. Hedin and S. Lundqvist, *Solid State Phys.*, v. 23 (Academic Press, New York, 1969), p. 1.
⁴³ M. S. Hybertsen and S. G. Louie, *Phys. Rev. B* **34**, 5390 (1986).
⁴⁴ R. W. Godby, M. Schlüter, and L. J. Sham, *Phys. Rev. B* **37**, 10159 (1988).
⁴⁵ M. Rohlfing, P. Krüger, and J. Pollman, *Phys. Rev. B* **48**, 17791 (1993).
⁴⁶ H. J. Monkhorst and J. D. Pack, *Phys. Rev. B* **13**, 5188 (1976).

- ⁴⁷ D. J. Chadi, P. H. Citrin, C. H. Park, D. L. Adler, M. A. Marcus, and H.-J. Gossmann, *Phys. Rev. Lett.* **79**, 4834 (1997).
- ⁴⁸ P. E. Blöchl, E. Smargiassi, R. Car, D. B. Laks, W. Andreoni, and S. T. Pantelides, *Phys. Rev. Lett.* **70**, 2435 (1993).
- ⁴⁹ H.-J. Sun, G. D. Watkins, F. C. Rong, L. Fotiadis, and E. H. Poindexter, *Appl. Phys. Lett.* **60**, 718 (1992).
- ⁵⁰ E. R. Weber, H. Ennen, U. Kaufmann, J. Windscheif, J. Schneider, and T. Wosinski, *J. Appl. Phys.* **53**, 6140 (1982).